7-9-2016

Rate-weakening drag during glacier sliding

Lucas K. Zoet
University of Wisconsin-Madison

Neal R. Iverson
Iowa State University, niverson@iastate.edu

AGU PUBLICATIONS

JGR

Journal of Geophysical Research: Earth Surface

RESEARCH ARTICLE

10.1002/2016JF003909

Key Points:
- A ring-shear device was used to study glacier slip with cavities over a stepped, rigid bed
- Basal drag decreased with sliding speed (rate weakening), contrary to stepped-bed theory
- Results motivate consideration of rate-weakening drag in glacier flow models

Supporting Information:
- Supporting Information SI

Correspondence to:
L. K. Zoet,
lzoet@wisc.edu

Citation:
Zoet, L. K., and N. R. Iverson (2016), Rate-weakening drag during glacier sliding, *J. Geophys. Res. Earth Surf.*, *121*, 1206–1217, doi:10.1002/2016JF003909.

Received 31 MAR 2016
Accepted 19 JUN 2016
Accepted article online 22 JUN 2016
Published online 9 JUL 2016

Rate-weakening drag during glacier sliding

Lucas K. Zoet[1,2] and Neal R. Iverson[2]

[1]Department of Geoscience, University of Wisconsin-Madison, Madison, Wisconsin, USA, [2]Department of Geological and Atmospheric Sciences, Iowa State University of Science and Technology, Ames, Iowa, USA

Abstract Accurately specifying the relationship between basal drag on a hard, rough glacier bed and sliding speed is a long-standing and central challenge in glaciology. Drag on a rigid bed consisting of steps with linear treads inclined upglacier—a good idealization for the bedrock morphology of some hard-bedded glaciers—has been considered in sliding theories but never studied empirically. Balancing forces parallel to step treads indicates that drag should be independent of sliding speed and cavity size and set by the limit-equilibrium condition sometimes called Iken's bound. In this study we used a large ring-shear device to slide ice at its pressure melting temperature across a stepped bed, over a range of steady sliding speeds (29–348 m yr^{-1}), and under a steady effective pressure (500 kPa). Contrary to expectation, drag decreased 42% with increasing sliding speed and cavity size. Experimental deviations from theory cannot explain this decrease in drag with increasing sliding speed (i.e., rate weakening). We suggest that stress bridging in ice between ice-bed contact zones and cavities causes stress gradients that require viscous deformation of ice to sustain stress equilibrium, so that contact zones can be at shear stresses below limit-equilibrium values. A parameter—linearly dependent on sliding speed—that scales the extent of ice deformation to areas of ice-bed contact allows the experimental drag relationship to be fitted with a simple sliding model. Rate-weakening drag has now been observed for two contrasting bed morphologies, stepped and sinusoidal, highlighting the need to consider such behavior in glacier flow models.

1. Introduction

Discharge of land-based glacier ice into the oceans is a major contributor to sea level rise, but large uncertainties associated with characterizing flow processes severely limit the accuracy of model predictions [*Stocker et al.*, 2013]. Glacier flow models with different objectives, such as characterizing glacial landscape evolution, suffer from the same limitation [e.g., *Egholm et al.*, 2009, 2012; *Herman et al.*, 2015]. As ice sheet and glacier models become more sophisticated through improved computational techniques, the continued use of primitive, and in some cases largely untested, constitutive equations will lead to progressively larger relative sources of error. Although efforts to incorporate more realistic constitutive relationships are ongoing [e.g., *Tsai et al.*, 2015; *Minchew et al.*, 2016], better empirical justification for them is clearly desirable.

Among the most important of these constitutive relationships are those used to characterize slip of wet-based glaciers over hard beds, which can result in fast glacier flow [e.g., *Kamb*, 1987; *Fowler*, 1979, 1987] and is essential for the bedrock erosion that is responsible for Alpine landscapes [*Pedersen and Egholm*, 2013; *Herman et al.*, 2015; *Koppes et al.*, 2015]. Although basal-slip rules have been the subject of long-term theoretical debate [*Weertman*, 1957, 1964; *Lliboutry*, 1968, 1979; *Kamb*, 1970; *Fowler*, 1986; *Schoof*, 2005], they are difficult to test empirically. More specifically, the relationship between sliding speed and basal drag is difficult to measure in the field because basal drag cannot be measured over appropriately short length scales and generally differs from the glacier driving stress [*Cuffey and Paterson*, 2010]. Efforts to use control methods to invert for basal drag from measured surface velocities are somewhat circular in this context because a direct, linear proportionality (as given by β^2 [e.g., *MacAyeal et al.*, 1995]) is usually assumed a priori between basal drag and sliding speed [*MacAyeal*, 1992; *Larour et al.*, 2014]. Moreover, knowledge of bed geometry at relevant scales is usually absent or poor. Scaled down experimental studies of sliding have usually failed either to reproduce temperate conditions, to measure the important effect of ice-bed separation, or to yield steady state relationships between drag and sliding speed (see *Zoet and Iverson* [2015] for a review).

A recently developed laboratory ring-shear device at Iowa State University allows sliding of temperate ice to be studied for the case of negligible regelation, a rigid bed with periodic roughness elements, and ice-bed separation [*Iverson and Petersen*, 2011]. The first complete suite of experiments with the device focused on slip over a sinusoidal bed [*Zoet and Iverson*, 2015; *Iverson and Zoet*, 2015]. These experiments provided a first

Figure 1. Stepped bed in the forefield of Castleguard Glacier, Alberta, Canada. The bedrock consists of subhorizontal limestone strata. Ice flow was from left to right. Photo by Tom Hooyer.

test and confirmation of the hypothesis that at increasingly large steady sliding speeds, steady drag on a sinusoidal bed increases, peaks, and then decreases over a wide range of speed [*Lliboutry*, 1968, 1979; *Fowler*, 1986, 1987; *Schoof*, 2005; *Gagliardini et al.*, 2007].

This so-called double-valued sliding relationship results from cavities that develop in the lees of undulations, so that only part of the adverse slope of the undulation immediately downstream is in contact with ice [*Lliboutry*, 1987; *Fowler*, 2010]. If sliding speeds are sufficiently small that a leeside cavity does not extend to the inflection point of the adverse slope of the undulation immediately downstream, increments in sliding speed and cavity size do not influence the maximum adverse bed slope in contact with ice. Thus, drag increases with sliding speed, as in models that do not consider ice-bed separation [e.g., *Nye*, 1969]. However, if cavities extend to the inflection point of the adverse slope downglacier, drag peaks and further increments in speed and cavity size will decrease the maximum adverse bed slope in contact with ice, causing the drag to decrease.

We expect this decrease in drag with increasing sliding speed—sometimes called rate weakening [*Marone*, 1998]—to occur beneath hard-bedded glaciers that have convex stoss surfaces, so that cavity growth reduces adverse bed slopes in contact with ice. The implications of such rate weakening at the bed are potentially major [*Schoof*, 2005], implying that, in response to an externally driven increase in glacier velocity, stabilizing viscous slip resistance may not operate over all or parts of glacier beds. The result could be either inertial glacier accelerations or, more likely, higher stresses on parts of glacier boundaries not subject to this effect, causing amplification of the increase in glacier speed.

A focus, however, on only sinusoidal beds or on more complicated geometries with only convex surfaces would be misguided. Although convex stoss surfaces on deglaciated bedrock are indeed common (e.g., roche moutonnées and whalebacks [*Benn and Evans*, 2010]), many stoss surfaces are close to planar (Figure 1). For example, in recently deglaciated forefields of hard-bedded glaciers, bedrock surface morphology is largely a result of subglacial erosion exploiting preexisting planes of weakness [*Hooyer et al.*, 2012; *Iverson*, 2012; *Anderson*, 2014]. In sedimentary rocks these planes of weakness are commonly planar bedding surfaces, and igneous and metamorphic rocks contain joint sets that commonly are nearly planar and orthogonal [*Krynine and Judd*, 1957]. Exploitation of these planes of weakness by subglacial erosion causes the stepped-bed morphology observed in some glacier forefields (Figure 1) [*Hallet and Anderson*, 1980; *Hooyer et al.*, 2012] and assumed in models of glacial erosion [*Röthlisberger and Iken*, 1981; *Iverson*, 1991, 2012; *Hallet*, 1996; *Zoet et al.*, 2013a; *Anderson*, 2014]. Thus, in considering constitutive rules for slip over

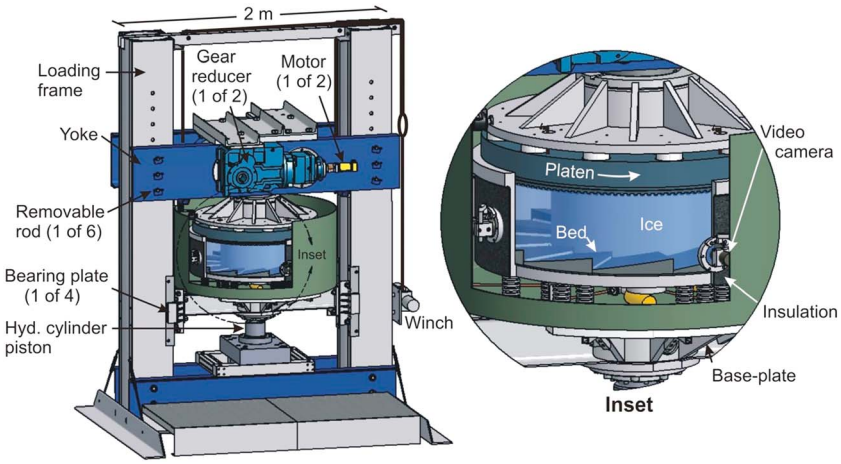

Figure 2. Device schematic used for sliding experiments. The inset details the sample chamber containing the stepped bed. An annular plate with teeth grips the ice ring at its upper surface and drags it across the bed and along smooth walls that confine the ice ring laterally.

hard beds, stepped beds should be considered as one idealized end-member of a continuum of forms, with sinusoidal beds as the other end-member.

A stepped bed with linear stoss surfaces is thought to result in a relation between sliding speed and drag that is distinct from that of a sinusoidal bed. *Iken* [1981] considered a stepped bed with water-filled cavities. She demonstrated that to sustain stress equilibrium for a given ice overburden pressure, water pressure could not exceed a threshold value dependent on the adverse slope of stoss surfaces. The corresponding upper limit of shear stress on the bed, for a given effective pressure and adverse bed slope, is sometimes called Iken's bound [e.g., *Schoof*, 2005]. This bound is assumed to be independent of sliding speed and cavity size because adverse bed slopes are uniform: the smaller contact areas between ice and stoss surfaces when cavities are large are exactly compensated, owing to the uniform slope, by the larger normal forces over these areas. Thus, once cavities develop on a stepped bed, rate-independent slip resistance that is dependent on effective pressure is expected (equivalent to "Coulomb friction" [e.g., *Schoof*, 2010]). In contrast, for the case of a sinusoidal bed the maximum adverse slope in contact with ice is smaller for progressively larger cavities, provided that they extend beyond the inflection points of adverse slopes, resulting in a reduction in drag at progressively higher speeds—the aforementioned rate weakening. Importantly, for both bed geometries, the maximum drag is set by the limit-equilibrium condition that depends on the adverse slopes of steps and the effective pressure and is independent of the ice rheology.

Herein we report the results of the first experimental study of ice slip over a stepped bed with leeward cavities. We find that although rate weakening for a stepped bed is less than that of a sinusoidal bed, it is still, contrary to expectation, significant. After exploring and discounting possible differences between the theory and experiments that might cause rate weakening when rate-independent slip is expected, we provide an explanation for how bed basal shear stress may attain values that are less than Iken's bound and thus decrease with sliding speed.

2. Methods

The device and protocol for these experiments were the same as for our experiments with a sinusoidal bed [*Zoet and Iverson*, 2015; *Iverson and Zoet*, 2015]. The device rotates a large ring of ice (0.9 m outside diameter, 0.2 m width, approximately 0.21 m thick) across a rigid bed under a constant effective pressure (Figure 2). The ring of ice, held in an aluminum chamber of *U*-shaped cross section, is gripped at its top by a toothed platen made of Delrin®, a polyoxymethylene, high-density plastic of low thermal conductivity that prevents slip of ice across the platen as it rotates. Rotation thus causes the bottom of the ice ring to slip over the bed. The device can accommodate unlimited slip displacement. The ice is held at its pressure-melting temperature by a glycol/water mixture that circulates around the ice chamber and regulates its temperature with a

precision of 0.01°K. Applied to the ice is a constant vertical stress that is maintained for the duration of the experiment. Meltwater produced during the experiment drains through 16 ports in the bed, keeping water pressure very near atmospheric. Because of the low water pressure, the effective stress is essentially equal to the vertical applied stress. A hydraulic ram supplies the vertical stress, kept by a servo to within 2% of the set-point value while allowing movement of the ram normal to the bed to accommodate changes in the ice-chamber volume. A displacement transducer measures vertical movement of the ram, tracking melt rates and changes in cavity size during sliding. In these experiments sliding speed is controlled while basal drag is measured during slip.

2.1. Bed

The stepped bed consists of 12 identical steps with adverse slopes of 8.4° and vertical lee surfaces (Figure 2). Each step has a length of 183 mm and a height of 27 mm at the centerline of the ice ring annulus. Because Iken's bound depends on the along-flow adverse bed slope, it is uniform, both longitudinally and radially, across the upstream facing surface of each step. Owing to the annular geometry, uniform adverse slopes require that step length and height decrease radially toward the inside wall of the ice chamber; decreases in slip speed toward the inside wall scale with decreases in step length and height. The bed is designed so that the combination of step length and low thermal conductivity is sufficient to render regelation negligible [*Zoet and Iverson*, 2015] and thereby isolate the effects of sliding by viscous creep for direct comparison with theories that neglect regelation. The bed, like the upper platen, is made of Delrin®, which has a thermal conductivity (0.33 $W\,m^{-1}\,°C^{-1}$) that is ~10 times smaller than that of most rocks. This bed material also has a very low coefficient of surface friction, μ, when ice at its melting temperature slips across it ($\mu < 0.02$). This low coefficient is important because zero surface friction is assumed in sliding theories, owing the thin water film that divides ice from rock.

In another experiment a flat, smooth bed of the same material is used to measure drag resulting from boundary effects unrelated to the bed roughness (dubbed the "background drag"), so that basal drag alone can be isolated in the experiments with a stepped bed. Also, applying different vertical stresses on the ice ring in this experiment allows for the measurement of an effective friction coefficient for the smooth, flat bed.

2.2. Procedure

An ice ring is constructed by crushing ice made from deionized water to create millimeter-scale ice grains. At a cold room temperature of −5°C, these grains are added to the sample chamber in a layer ~15 mm thick and then flooded with deionized water, which creates ice with more or less random crystal orientations. Once the layer is frozen, this procedure is repeated until the chamber is full of ice. During ice deformation associated with sliding, ice recrystallizes and develops fabrics like that of temperate ice at glacier beds [*Iverson and Petersen*, 2011; *Zoet and Iverson*, 2015]. During construction of the ice ring, beads threaded onto strings suspended vertically are frozen in place 3.0 cm from the inner and outer walls to be used as displacement markers to assess strain and melting at the wall off the ice chamber. Once the ice ring is constructed, the upper platen is lowered into contact with the ice ring, and the platen's teeth are frozen into the ring's upper surface. A vertical stress (approximately 250 kPa) is then applied, which is approximately 50% of the vertical stress to be applied during sliding. Simultaneously, the cold room temperature is set to 0°C, and the temperature of the circulating fluid in the surrounding bath is raised to a fraction of a degree above the pressure-melting temperature. The ice ring is kept at rest under these conditions, while heat is conducted into its interior. The ice temperature is monitored until it reaches the pressure-melting temperature indicated by 22 thermistors (precision of ~0.01°K) embedded in the inner and outer walls and the bed of the device. Ensuring that the interior of the ice ring is at the pressure-melting temperature requires approximately 6 days because of the need to melt ice while conducting heat inward. The vertical stress is then raised to approximately 500 kPa. A corresponding sudden decrease in the ice temperature recorded by thermistors results from this sudden increase in vertical stress, further indicating that the ice is at the pressure-melting temperature.

Rotation of the upper platen at a constant velocity causes slip of the ice ring over the bed, while shear stress is measured. Initiation of sliding begins a transient phase as cavity geometry and basal shear stress adjust to the sliding speed. This transient phase can last 2–14 days depending on the magnitude of the change in sliding speed and the initial size of cavities. Eventually, shear stress varies minimally about a steady value (Figure 3), and the displacement transducer monitoring movement of the hydraulic ram indicates that cavities have

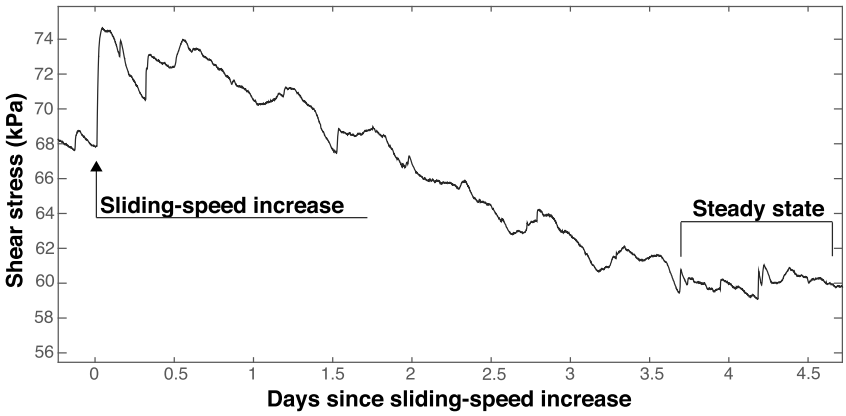

Figure 3. Transient shear stress. Evolution of shear stress to a steady state value after a sliding-speed increase from 58 to 116 m yr^{-1} at an effective pressure of 500 kPa.

reached a steady volume. Sliding speed is then increased again, and the process is repeated. In other cases, sliding speed is stepped down. Data presented are from two different experiments that collectively lasted 3.5 months.

2.3. Cavity Geometry

When an experiment is completed, the upper platen is separated from the ice ring, and the ice ring is extracted with a winch for analysis. Shear strains, as indicated by the relative displacements of beads in initially vertical strings, are measured. The ice ring is then inverted so that its sole faces upward, and a jig is used to measure the basal topography and thereby determine the cavity geometry. Elevation measurements are made at 280 locations along the circumference of the ring at five radial positions that incrementally span most of the width of the ring.

The cavity geometry measured after an experiment records the steady geometry at only the final sliding speed. To determine cavity geometry at steady speeds earlier in the experiments, when no direct measurement of geometry was possible, the measured cavity geometry at the ends of experiments was fitted with a model of step cavities [*Kamb*, 1987], and the fitted model was used to predict cavity geometry earlier in the experiment (Appendix A). The cavity volumes associated with these predictions were then evaluated independently using the record of ice-chamber volume provided by the movement of the vertical ram. To separate changes in ice-chamber volume due to changes in cavity size from those due to melting of ice and water drainage, uniform rates of ice-ring thinning during periods of steady shear stress and cavity size were attributed to melting and interpolated across periods of transient cavity adjustment. The cavity model of *Kamb* [1987] was also fitted to cavity geometry and sliding speed measured at different radial positions at the ends of experiments.

3. Results

Immediately after an increase in sliding speed, shear stress always abruptly rose (Figure 3). After a period of several days, sliding displacement was sufficient to allow cavities to attain a steady size, indicated by the record of ice-chamber volume. Over the same period, shear stress changed but, as noted, eventually oscillated at high frequency about a steady value (Figure 3).

Over the range of experimental sliding speeds (29–348 m yr^{-1}) at different times in the experiments, steady state cavities spanned most of stoss surfaces but with lengths that increased with speed (Figure 4a). The same was true for cavities measured across the width of the bed, with lengths that increased radially outward with increases in step height and sliding speed (Figure 4b). Heights of the measured cavities were consistently smaller immediately downstream of the step edge than modeled values (Appendix A) by an average of approximately 2% (Figure 4). Differences between the measured and theoretical cavity lengths were also small, with no systematic tendency to underestimate or overestimate lengths. Fitting the cavity model to cavity roofs measured at various radial positions (283, 316, 350, 383, and 416 mm, referenced to the rotation

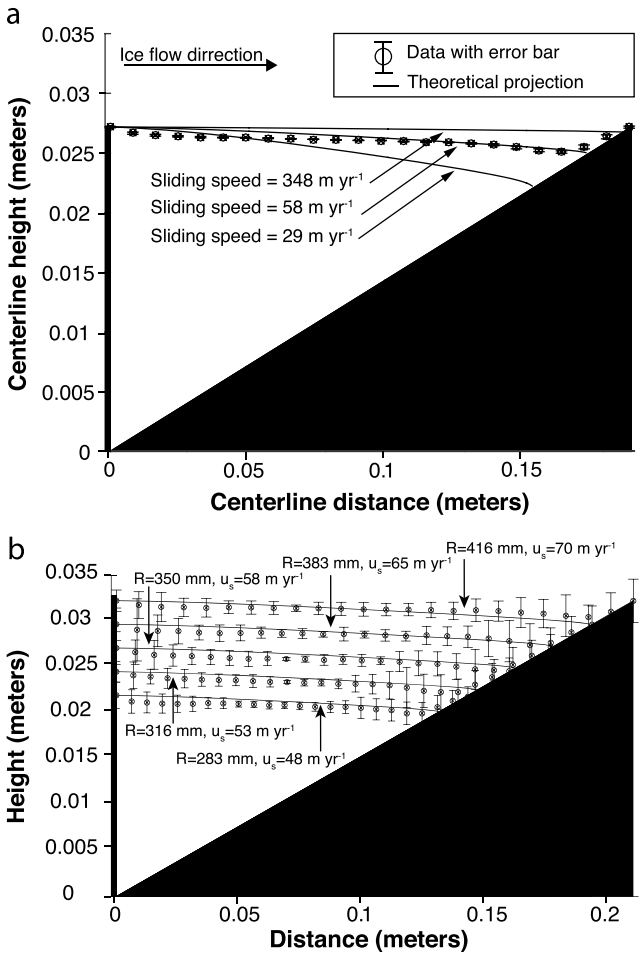

Figure 4. Measured and predicted cavities at the bed (vertically exaggerated) due to sliding. (a) Predicted longitudinal profiles of cavities at three different sliding speeds at the ice-chamber centerline from the theory of *Kamb* [1987]. Predicted cavity profile at a sliding speed of 58 m yr^{-1} is compared with mean measurements of the roofs of 12 cavities (circles with error bars). Sliding speeds of 29 and 348 m yr^{-1} are the bounding cavity sizes for the experiment. Error bars represent ± 1σ. (b) Longitudinal profiles of cavities at five radial distances from the ice-chamber center (in millimeters) and associated sliding speeds. Cavity geometry was both measured directly (circles with error bars) and fitted using the theory of *Kamb* [1987]. Error bars indicate ± 1σ based on measurements of 12 different cavities.

axis of the device) at the ends of experiments (Figure 4b) yielded misfits of the actual and predicted values of −0.74, −1.3, 1.17, −0.55, and 1.5%, respectively. The average absolute misfit was approximately 1%. This good correspondence provides confidence in comparisons of our three-dimensional data with predictions of two-dimensional sliding theories.

Cavity size estimates at various times in the experiments were checked independently by comparing modeled cavity volumes with the record of ice-chamber volume. For the final sliding speed of 58 m yr^{-1} (Figure 4a), cavity volume estimates from the ice-chamber volume were within 3% of values measured directly from basal topography, as well as those predicted using the cavity model (Appendix A). The misfit between cavity expansion volumes and predicted cavity volumes for additional sliding speeds of 29, 116, 232, and 348 m yr^{-1} were 13, 5, 7, and 8%, respectively.

Importantly, at progressively higher sliding speeds measured values of steady state shear stresses supported by the bed decreased (Figure 5). Cavities formed at the lowest applied sliding speed, so over no part of the range of sliding speed studied did shear stresses increase with speed. All measured shear stresses were below Iken's bound (83 kPa, based on the adverse bed slope, the 500 kPa effective pressure, and the measured background drag; Figure 5). Although this bound is a necessary requirement for sustaining stress equilibrium, shear stress did not reside at the bound as expected. A change in sliding speed from 29 to 348 m yr^{-1} (a factor of 12 increase) resulted in a 42% decrease in the measured steady shear stress from 76 to 44 kPa. Background values of drag recorded in a separate experiment with the flat bed were consistently small (~9 kPa) and independent of sliding speed (Figure 5), indicating that boundary conditions of the experimental setup (e.g., bed and wall friction) were not velocity dependent and so were not the cause of the shear stress decrease.

4. Discussion

The decrease in shear stress with increasing sliding speed does not match the rate-independent response expected if the system had simply remained at limiting equilibrium (Iken's bound) at all speeds. An important question that requires thorough exploration is whether this rate weakening was an experimental artifact or an effect more fundamental.

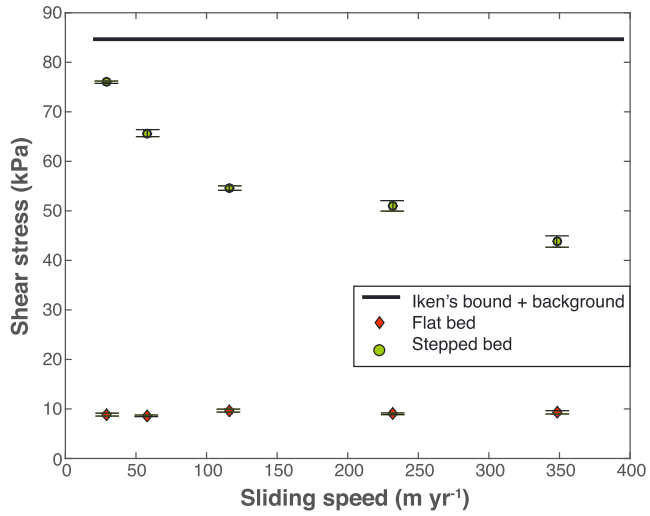

Figure 5. Steady shear stress as function of sliding speed for a stepped and flat bed. Error bars indicate ± 1σ once a time-averaged steady shear stress was reached. The solid black line is Iken's bound calculated for a bed slope of 8.4°, added to the background drag for a flat bed.

4.1. Friction

A decrease in the friction coefficient, μ, between ice and the bed with an increase in normal stress over the reduced ice-bed contact area that accompanies cavity growth would reduce shear stress with increased sliding speed. For ice sliding over a flat bed at an effective stress of 500 kPa, as in the experiments, $\mu = 0.018 \pm 0.002$, whereas experiments conducted at 1000 kPa indicate that $\mu = 0.016 \pm 0.001$. Even if this slight reduction in μ is considered to be significant, it yields only ~1 kPa reduction in shear stress, bearing in mind that the effect of increases in normal stress between ice and the bed on the frictional component of shear stress are compensated by the smaller area over which the normal stress acts.

4.2. Flexure or Rotation of the Bed

Another possible effect in the experiment that would have reduced Iken's bound was a decrease in the adverse slopes of bed steps as the cavities grew. Rotation or elastic flexure of bed steps as cavity growth concentrated normal stresses near the downstream edges of steps could have caused a decrease in adverse bed slope. Under the vertical stress of the experiment (500 kPa), a reduction in adverse slopes from 8.4° to 4.0° would have been required to reduce Iken's bound sufficiently to produce the observed decrease in shear stress. The construction of the bed pieces that comprise each step ensures that they effectively "lock" together, so there was no possibility of any rigid rotation of a bed step. Thus, only elastic flexure of the bed could have caused a change in slope angle. Over the range of cavity sizes in the experiments (Figure 4a), the area of contact between ice and a bed step was reduced from 52 cm^2 to approximately 20 cm^2, causing an approximately threefold increase in normal stress. With a Young's modulus for the Delrin steps at 0°C of approximately 2.4 GPa [*Dupont*, 2003], this increase in load would have produced a relative shortening of approximately 0.06 mm from the upstream to the downstream edges of the steps. This shortening will have reduced the adverse slope angle by ~0.02°, thereby reducing Iken's bound by 0.2%—far less than the decrease observed (Figure 5).

4.3. Three-Dimensional Bed

Although we expect the radial geometry of the bed to have affected measured values of shear stress, observations of cavity size and bead columns provide no evidence of an effect that would have led to rate weakening. Asymmetric cavity development and associated movement of ice along paths that deviated from being circumferential could have conceivably caused weakening as cavities grew. However, the observed radial cavity geometries varied on average 1% from values based on two-dimensional theory (Appendix A) and in no systematic pattern. Furthermore, beads in initially vertical columns did not move at a systematic angle to the circumferential trend. A slight displacement of bead columns toward the walls, driven by melting along the sides of the ice ring, was symmetric about the ice-chamber centerline and orders of magnitude smaller than the circumferential displacement of ice.

4.3.1. Alternative Hypothesis

None of these experimental deviations from the theory can explain the observed 42% decrease in the drag. The data, therefore, indicate that sliding at progressively higher speeds occurred at steady shear stresses increasingly below the limit-equilibrium value set by Iken's bound.

First, we reconsider the rationale for why slip over a stepped bed at a particular effective pressure should occur at a single, rate-independent shear stress (Iken's bound) once water in cavities fully drowns lee surfaces. Slip at that state of limit equilibrium requires that downglacier and upglacier forces parallel to

the adverse slopes of steps are exactly equal. For the tilted-staircase bed that *Iken* [1981] considered, in which lee surfaces are perpendicular to planar stoss surfaces, this is precisely the same condition at which ice separates from lee surfaces and cavities form:

$$\tau_c = N \tan\beta, \tag{1}$$

where τ_c is the critical shear stress at Iken's bound, N is the effective pressure, and β is the adverse bed slope. Larger cavities result in smaller zones of ice-bed contact and higher normal stresses there, but these higher normal stresses do not change Iken's bound because resultant shear stresses are acting over exactly compensating smaller areas with the same adverse slope. Thus, as long as cavities extend fully across the leesides of steps, as they did for the measured shear stresses plotted in Figure 5, and adverse slopes are uniform, slip will seemingly occur at a single shear stress set by Iken's bound, regardless of sliding speed.

However, closer consideration of contact areas between ice and rock indicates that shear stresses smaller than Iken's bound are possible, even if water in cavities fully drowns lee surfaces. This is because the simple model neglects that stresses on zones of ice-bed contact, even if they are planar, will not be uniform. For example, study of ice normal stresses on stepped beds, where water-filled cavities are present, indicates that near the upstream and downstream edges of zones of ice-bed contact, normal stresses are larger than elsewhere, as highlighted in models of bedrock quarrying [e.g., *Iverson*, 1991; *Hallet*, 1996; *Hildes et al.*, 2004]. These stress concentrations result from their proximity to the cavity, where the water pushes upward on the cavity roof under a pressure smaller than the ice-overburden pressure; resultant bridging effects in the ice cause stress concentrations on immediately adjacent zones of ice-bed contact [*Murray and Clarke*, 1995]. Critically, if normal stresses vary along a zone of uniformly sloping ice-bed contact, stresses parallel to the overall slope of the bed (0° in the experiments) will also vary along the contact requiring longitudinal stress gradients and associated viscous deformation of ice to sustain stress equilibrium. The result will be that some of the ice-bed contact will be at shear stresses controlled by the deformation resistance of ice. These shear stresses will be less than Iken's bound.

Our hypothesis is that with increasingly small zones of ice-bed contact the stress gradients due to local deviations from Iken's bound increase and that this effect can explain decreases in bed shear stresses with increasing sliding speed and cavity size. To formalize this idea, we consider a simple treatment of sliding that follows *Weertman*'s [1964] analysis but with certain parameters conceptualized differently for this problem. We neglect any component of slip that may have resulted from pressure-induced melting, as justified in Appendix B. Also, despite ice-bed stresses in excess of those considered in sliding theories [e.g., *Nye*, 1969; *Kamb*, 1970], we see no evidence of ice fracturing in the character of shear-stress time series from experiments or from postexperimental observations of the ice ring. Thus, only viscous flow of ice is considered.

Weertman [1957, 1964] suggested that under these conditions sliding speed is proportional to the size of the obstacle, l; the strain rate, $\dot{\varepsilon}$; and a "factor of proportionality," b:

$$u_s = \dot{\varepsilon} l b. \tag{2}$$

Strain rate, $\dot{\varepsilon}$, can be estimated from the local stress on an obstacle and then applied over a length proportional to l as scaled by b. Although heuristic, b is of O (1) and sets the ice volume over which a given sized obstacle induces enhanced deviatoric stresses and ice creep. A small bump causes strain over a small volume, and thus, the resultant slip displacement is small. The strain rate follows from the flow law of ice:

$$\dot{\varepsilon} = \left(\frac{\tau_l}{B}\right)^n, \tag{3}$$

where τ_l is the local stress on the obstacle, $n = 3$, and B is the viscosity parameter obtained from the cavity-fitting procedure (described in Appendix A).

If appropriate allowances are made for cavity size, τ_l in the experiments can be estimated from the measured bed shear stress, τ_b. If λ is taken to be the length of steps along the ice-chamber centerline (0.183 m), the three-dimensionality of the bed is neglected, and w is the step width, then the shear force on the bed is $\tau_b w \lambda$. Cavities can be thought of as reducing both the effective length, l_e, and effective height, h_e, of the bed steps, such that both of these quantities depend on the sliding speed. Their variation with sliding speed is known

Table 1. Values of Sliding Speed and Associated Values of b_e, l_e, and l_e b_e

Speed (m yr^{-1})	b_e	l_e (cm)	l_e b_e (cm)
29	0.8	3.8	3.0
58	1.1	2.6	2.9
116	1.8	1.7	3.0
232	2.0	1.1	2.2
348	2.9	0.8	2.3

from the experiments because cavity size is known as a function of sliding speed. The local shear stress, τ_l, on zones of ice-bed contact is thus

$$\tau_l = \frac{\tau_b w \lambda}{w h_e}, \tag{4}$$

Similarly adjusting equation (2) by replacing l with l_e, noting that $l_e = h_e (tan\,\beta)^{-1}$, and importantly, replacing b with an effective value, b_e, which varies with sliding speed and cavity size, yields

$$u_s = \dot{\varepsilon} \frac{h_e b_e}{tan\,\beta}. \tag{5}$$

This equation, together with equations (3) and (4), provides relationships for bed shear stress as a function of sliding speed:

$$\tau_b = \left(\frac{u_s tan\,\beta}{h_e b_e}\right)^{1/n} \frac{B h_e}{\lambda}, \tag{6}$$

$$\tau_b = \left(\frac{u_s}{l_e b_e}\right)^{1/n} \frac{B l_e tan\,\beta}{\lambda}. \tag{7}$$

Equations (6) and (7) are equivalent, but equation (7) has been written in terms of l_e b_e. All variables in this equation can be measured or estimated other than b_e. If for each sliding speed and cavity size from the experiment, b_e is determined, it increases by a factor of approximately 4 (Table 1), as cavities grow with sliding speed, and ice-bed contact areas shrink by approximately a factor of 4. Also shown in Table 1 are values of the product, l_e b_e, a measure of the length scale over which ice is undergoing enhanced creep during sliding. Unsurprisingly, values of l_e b_e are smaller at higher sliding speeds when zones of ice-bed contact and hence l_e are smaller. However, owing to the larger values of b_e if contact areas are small, l_e b_e does not decrease proportionally with decreasing contact area. We attribute this trend to longitudinal stress gradients in zones of ice-bed contact that are larger when these zones are smaller. Thus, when contact zones are small, resultant enhanced creep spans an ice thickness that is large relative to the ice-bed contact zone, so b_e values are larger. Fitting a straight line to the experimental relationship between b_e and sliding speed (Table 1) and using that linear fit in equation (6) illustrate how this dependence on b_e accounts for the observed rate weakening (Figure 6).

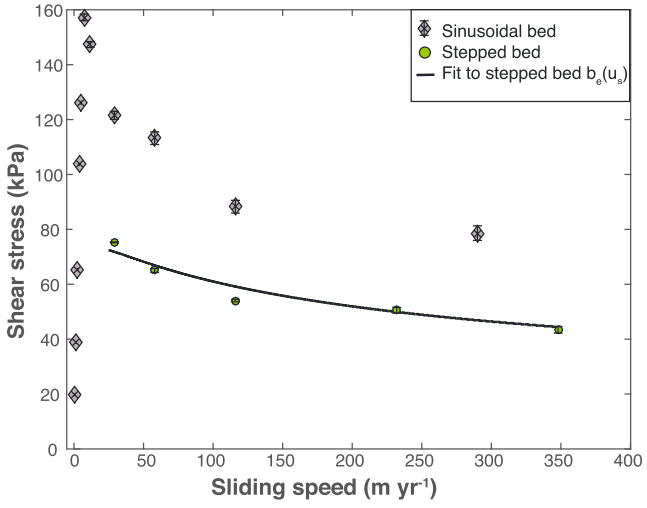

Figure 6. Steady shear stress as a function of sliding speed for a stepped and sinusoidal bed. Shear stresses for the stepped bed (circles) are compared with predicted values indicated by equation (6) (black line) for b_e values that are a linear function of sliding speed. Measured shear stresses for a sinusoidal bed [*Zoet and Iverson*, 2015] are shown with diamonds. All error bars indicate ± 1σ.

The distribution of shear strain across the thickness of the ice ring provides a check on the values of l_e b_e derived from the analysis. The relative displacements of beads in initially vertical columns in the ice show the tendency for more than 90% of shear strain to be focused in the lowermost 3.0 cm of the ice ring (Figure 7)—a value close to computed values of l_e b_e.

Comparing the experimental relationship between drag and sliding speed for the stepped bed with that of a sinusoidal bed [*Zoet and Iverson*, 2015] illustrates the effects of bed geometry on drag. Shear stresses were significantly higher for the sinusoidal bed because its maximum adverse bed slope was higher than for the stepped bed (27.6° versus 8.4°). The rising limb of the curve for the case of

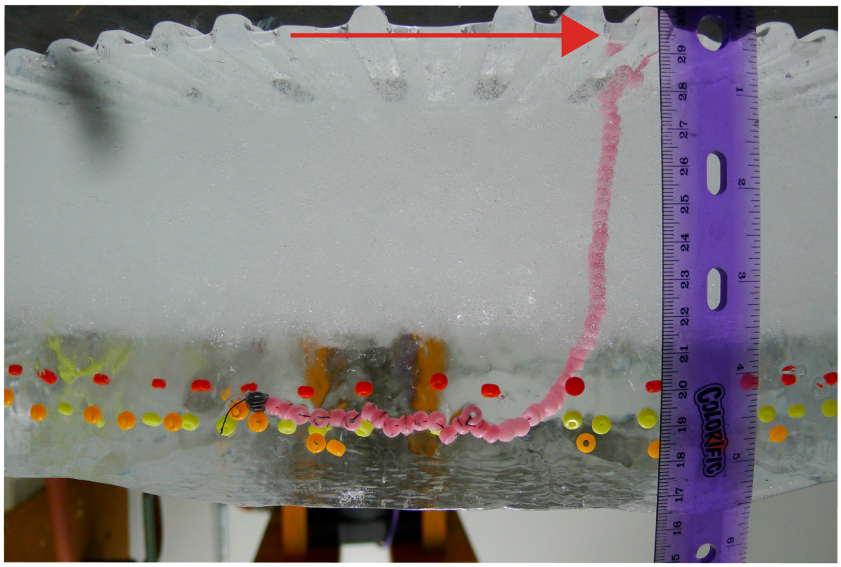

Figure 7. Ice deformation. Along-flow view of the ice ring at the end of an experiment, showing displacement of beads (pink) that were in a vertical column prior to sliding. The upper surface was gripped and displaced to the right (as denoted by the arrow) as ice slid across the bed. Note that left side of the scale is in centimeters. Nonpink beads were used to track sliding displacement and were not initially in vertical columns. Clear ice in the lowermost 40% of the ice ring reflects recrystallization during ice deformation that purged air bubbles from the ice.

the stepped bed is absent because tests were not conducted at sufficiently low sliding speeds to prevent cavity growth, owing to the vertical lee surfaces of bed steps that cause cavities to form at very low speeds. More importantly, comparison of the two sets of results indicates that about half of the rate weakening observed for a sinusoidal bed may be attributable to the dependence of b_e on sliding speed, whereas the remaining decrease may reflect the progressively smaller adverse slopes of ice-bed contact areas, as cavities increase their sizes with increasing sliding speed [*Schoof*, 2005; *Zoet and Iverson*, 2015]. A reasonable inference, therefore, based on the results with the stepped bed, is that some of the rate weakening in the sinusoidal-bed case was due to longitudinal stress gradients related to bridging effects between cavities and ice-bed contact zones.

The granular materials used to simulate fault gouge regularly demonstrate rate-weakening slip that can be parameterized within the context of rate-and-state friction [e.g., *Scholz*, 2002]. Empirically derived rate-and-state friction rules are commonly used to characterize frictional slip on faults [*Dieterich*, 1979; *Ruina*, 1983] and in some instances glaciers [*Zoet et al.*, 2013b]. Although frictional slip of faults and slip of hard-bedded glaciers both can exhibit rate weakening, disparate processes are responsible for the weakening. Rate weakening during slip of glaciers over hard beds results from ice-bed separation, whereas rate weakening during frictional fault slip requires an adjustment between asperity contacts on rock surfaces [*Scholz*, 2002].

5. Implications

These results, when considered with our previous experimental results [*Zoet and Iverson*, 2015] (Figure 6), indicate that for the two bounding geometries of adverse slopes, hard beds may become increasingly "slippery" as sliding speed increases. How important is this effect likely to be for the more complicated hard beds of real glaciers? Various complexities are not replicated by the experiments: regelation, drag caused by debris in ice [*Hallet*, 1981; *Cohen et al.*, 2005], transient freezing on parts of the bed [*Robin*, 1976], and the variable sizes and shapes of obstacles, including their three-dimensionality. For the case in which drag associated with debris-bed friction is minor, considering the last of these is probably the most important for assessing rate-weakening drag. *Schoof* [2005] theoretically considered two-dimensional, arbitrary bed geometries and demonstrated the rate-weakening effect. Others have noted that a population of large obstacles could eliminate rate weakening [e.g., *Fowler*, 1987; *Lliboutry*, 1987], but this conjecture may be unrealistic because these large obstacles would need to have steeper adverse slopes than obstacles with cavities [*Schoof*, 2005].

A bigger uncertainty may stem from the three-dimensionality of real glacier beds. The extent to which obstacles with finite widths produce cavities capable of drowning adverse sloping surfaces immediately downglacier is highly uncertain and dependent on both the sizes of cavities and three-dimensional geometry of the bed surface. Given that bedrock lithology and jointing have a major influence on bed-surface morphology (e.g., Figure 1) by controlling bedrock erosion patterns [e.g., *Hooyer et al.*, 2012], the drag relationship for basal slip may well be sensitive to the geologic setting.

Despite the differences between bed idealizations—required of both experiments and sliding models—and the more complicated geometries of glacier beds, we find the theoretical and experimental evidence for rate-weakening drag to be sufficiently compelling to, at a minimum, warrant further study. Some of the uncertainties of its application to real glaciers could be narrowed through detailed morphologic study of the forefields of hard-bedded glaciers. Moreover, experimenting with the effects of rate-weakening constitutive rules in glacier models may help explain aspects of flow dynamics and glacial geomorphic observations that are difficult to explain otherwise. The recognition that some glaciers generate basal seismicity caused by stick slip—a phenomenon that requires rate-weakening drag—provides still more motivation for such study [*Zoet et al.*, 2012; *Allstadt and Malone*, 2014].

6. Conclusions

Over a wide range of increasing sliding speed (29–348 m yr^{-1}), steady drag on a bed consisting of steps with linear, inclined treads decreased by 42%, owing to growth of leeward cavities. This decrease in drag was far larger than can be accounted for by experimental deviations from theory. Thus, these data indicate that, despite cavities, viscous creep of ice past bed obstacles during sliding can occur at a shear stress—averaged over the bed area—that is below Iken's bound and that this shear stress decreases progressively as zones of ice-bed contact become smaller. As a working hypothesis, we suggest that stress bridging in ice between contact zones and cavities causes stress gradients that require viscous deformation of ice to sustain stress equilibrium. Contact areas can thus be at shear stresses less than limit-equilibrium values and controlled by the deformation resistance of ice. Stress gradients span broader areas relative to shrinking zones of ice-bed contact as cavities grow, an effect we represent with a scaling parameter, b_e, which if allowed to increase linearly with sliding speed, enables the experimental drag relationship to be fitted with a simple sliding model.

Comparison of drag data of this study with experimental data from a sinusoidal bed indicates that larger decreases in drag measured for a sinusoidal bed may have been partly a result of this ice-bridging effect. Experimental demonstration of rate-weakening drag for both bed types—end-members in the continuum of along-flow bed-surface morphologies—provides motivation for experimenting with rate-weakening drag in glacier flow models.

Acknowledgments
We thank T. Herrman and D. Jones of the U.S. Department of Energy Ames Laboratory for their help designing and fabricating the device. Construction and use of the device were made possible by grants from the U.S. National Science Foundation: ANT-0618747 and EAR-1023586. The data from these experiments are archived at the University of Wisconsin-Madison and can be obtained from the following link: https://uwmadison.box.com/s/tqxim7gs0jal9unqwy1qweydcukvgm1j.

References

Allstadt, K., and S. D. Malone (2014), Swarms of repeating stick–slip icequakes triggered by snow loading at Mount Rainier volcano, *J. Geophys. Res. Earth Surf.*, *119*, 1180–1203, doi:10.1002/(ISSN)2169-9011.

Anderson, R. S. (2014), Evolution of lumpy glacial landscapes, *Geology*, *42*, 679–682, doi:10.1130/G35537.1.

Benn, D. I., and D. J. Evans (2010), *Glaciers and Glaciation*, 2nd ed., Oxon. Hodder Education, London.

Cohen, D., N. R. Iverson, T. S. Hooyer, U. H. Fischer, M. Jackson, and P. L. Moore (2005), Debris-bed friction of hard-bedded glaciers, *J. Geophys. Res.*, *110*, F02007, doi:10.1029/2004JF000228.

Cuffey, K. M., and W. S. B. Paterson (2010), *The Physics of Glaciers*, 4th ed., Academic Press, Oxford.

Dieterich, J. (1979), Modeling of rock friction. 1. Experimental results and constitutive equations, *J. Geophys. Res.*, *84*, 2161–2168, doi:10.1029/JB084iB05p02161.

Dupont (2003), Design information for Delrin®, 1–37.

Egholm, D., S. Nielsen, V. K. Pedersen, and J. Lesemann (2009), Glacial effects limiting mountain height, *Nature*, *460*, 884–887, doi:10.1038/nature08263.

Egholm, D. L., V. K. Pedersen, M. F. Knudsen, and N. K. Larsen (2012), On the importance of higher order ice dynamics for glacial landscape evolution, *Geomorphology*, *141–142*, 67–80, doi:10.1016/j.geomorph.2011.12.020.

Fowler, A. C. (1979), A mathematical approach to the theory of glacier sliding, *J. Glaciol.*, *23*, 131–141, doi:10.3198/1979JoG23-89-131-141.

Fowler, A. C. (1986), A sliding law for glaciers of constant viscosity in the presence of subglacial cavitation, *Proc. R. Soc. Lond.*, *407*, 147–170, doi:10.1098/rspa.1986.0090.

Fowler, A. C. (1987), Sliding with cavity formation, *J. Glaciol.*, *33*, 255–267, doi:10.3198/1987JoG33-115-255-267.

Fowler, A. C. (2010), Weertman, Lliboutry and the development of sliding theory, *J. Glaciol.*, *56*, 965–972, doi:10.3189/002214311796406112.

Gagliardini, O., D. Cohen, P. Råback, and T. Zwinger (2007), Finite-element modeling of subglacial cavities and related friction law, *J. Geophys. Res.*, *112*, F02027, doi:10.1029/2006JF000576.

Hallet, B. (1981), Glacial abrasion and sliding: Their dependence on the debris concentration in basal ice, *Ann. Glaciol.*, *2*, 23–28, doi:10.3189/172756481794352487.

Hallet, B. (1996), Glacial quarrying: A simple theoretical model, *Ann. Glaciol.*, *22*, 1–8, doi:10.3198/1996AoG22-1-1-8.
Hallet, B., and R. S. Anderson (1980), Detailed glacial geomorphology of a proglacial bedrock area at Castleguard Glacier, Alberta, Canada, *Z. Gletscherk. Glazialgeol.*, *16*, 171–184.
Herman, F., O. Beyssac, M. Brughelli, S. N. Lane, S. Leprince, T. Adatte, J. Lin, J. Avouac, and S. Cox (2015), Erosion by an Alpine glacier, *Science*, *350*, 193–195, doi:10.1126/science.aab238.
Hildes, D. H. D., G. K. C. Clarke, G. E. Flowers, and S. J. Marshall (2004), Subglacial erosion and englacial sediment transport modelled for North American ice sheets, *Quat. Sci. Rev.*, *23*, 409–430, doi:10.1016/j.quascirev.2003.06.005.
Hooyer, T. S., D. Cohen, and N. R. Iverson (2012), Control of glacial quarrying by bedrock joints, *Geomorphology*, *153–154*, 91–101, doi:10.1016/j.geomorph.2012.02.012.
Iken, A. (1981), The effect of the subglacial water pressure on the sliding velocity of a glacier in an idealized numerical model, *J. Glaciol.*, *27*, 407–421, doi:10.3198/1981JoG27-97-407-421.
Iverson, N. R. (1991), Potential effects of subglacial water-pressure fluctuations on quarrying, *J. Glaciol.*, *37*, 27–36, doi:10.3198/1991JoG37-125-27-36.
Iverson, N. R. (2012), A theory of glacial quarrying for landscape evolution models, *Geology*, *40*, 679–682, doi:10.1130/G33079.1.
Iverson, N. R., and B. Petersen (2011), A new laboratory device for study of subglacial processes: First results on ice-bed separation during sliding, *J. Glaciol.*, *57*, 1135–1146, doi:10.3189/002214311798843458.
Iverson, N. R., and L. K. Zoet (2015), Experiments on the dynamics and sedimentary products of glacier slip, *Geomorphology*, *244*, 121–134, doi:10.1016/j.geomorph.2015.03.027.
Kamb, B. (1970), Sliding motion of glaciers: Theory and observation, *Rev. Geophys. Space Phys.*, *8*, 673–728, doi:10.1029/RG008i004p00673.
Kamb, B. (1987), Glacier surge mechanism based on linked cavity configuration of the basal water conduit system, *J. Geophys. Res.*, *92*, 9083–9100, doi:10.1029/JB092iB09p09083.
Koppes, M., B. Hallet, E. Rignot, J. Mouginot, J. S. Wellner, and K. Boldt (2015), Observed latitudinal variations in erosion as a function of glacier dynamics, *Nature*, *526*, 100–103, doi:10.1038/nature15385.
Krynine, D. P., and W. R. Judd (1957), *Principles of Engineering Geology and Geotechnics*, McGraww-Hill, New York.
Larour, E., J. Utke, B. Csatho, A. Schenk, H. Seroussi, M. Morlighem, E. Rignot, N. Schlegel, and A. Khazendar (2014), Inferred basal friction and surface mass balance of the Northeast Greenland Ice Stream using data assimilation of ICESat (Ice Cloud and land Elevation Satellite) surface altimetry and ISSM (Ice Sheet System Model), *Cryosphere*, *8*, 2335–2351, doi:10.5194/tc-8-2335-2014.
Lliboutry, L. (1968), General theory of subglacial cavitation and sliding of temperate glaciers, *J. Glaciol.*, *7*, 21–58.
Lliboutry, L. (1979), Local friction laws for glaciers: A critical review and new openings, *J. Glaciol.*, *23*, 67–95.
Lliboutry, L. (1987), Realistic, yet simple bottom boundary conditions for glaciers and ice sheets, *J. Geophys. Res.*, *92*, 9101–9109, doi:10.1029/JB092iB09p09101.
MacAyeal, D. R. (1992), The basal stress distribution of Ice Stream E, Antarctica, inferred by control methods, *J. Geophys. Res.*, *97*, 595–603, doi:10.1029/91JB02454.
MacAyeal, D. R., R. A. Bindschadler, and T. A. Scambos (1995), Basal friction of Ice Stream E, west Antarctica, *J. Glaciol.*, *41*, 247–262, doi:10.3198/1995JoG41-138-247-262.
Marone, C. (1998), Laboratory-derived friction laws and their application to seismic faulting, *Annu. Rev. Earth Planet. Sci.*, *26*, 643–696, doi:10.1146/annurev.earth.26.1.643.
Minchew, B., M. Simons, H. Bjornsson, F. Palsson, M. Morlighem, H. Seroussi, E. Larour, and S. Hensley (2016), Plastic bed beneath Hofsjökull Ice Cap, central Iceland, and the sensitivity of ice flow to surface meltwater flux, *J. Glaciol.*, *62*, 1–12, doi:10.1017/jog.2016.26.
Murray, T., and G. K. C. Clarke (1995), Black-box modeling of the subglacial water system, *J. Geophys. Res.*, *100*, 10,231–10,245, doi:10.1029/95JB00671.
Nye, J. (1969), A calculation on the sliding of ice over a wavy surface using a Newtonian viscous approximation, *Proc. R. Soc. Lond.*, *311*, 445–467, doi:10.1098/rspa.1969.0127.
Pedersen, V. K., and D. L. Egholm (2013), Glaciations in response to climate variations preconditioned by evolving topography, *Nature*, *493*, 206–210, doi:10.1038/nature11786.
Robin, G. Q. (1976), Is the basal ice of a temperate glacier at the pressure melting point?, *J. Glaciol.*, *16*, 183–196, doi:10.3198/1976JoG16-74-183-196.
Röthlisberger, H., and A. Iken (1981), Plucking as an effect of water-pressure variations at the glacier bed, *Ann. Glaciol.*, *2*, 57–62, doi:10.3189/172756481794352144.
Ruina, A. (1983), Slip instability and state variable friction laws, *J. Geophys. Res.*, *88*, 10,359–10,370, doi:10.1029/JB088iB12p10359.
Schoof, C. (2005), The effect of cavitation on glacier sliding, *Proc. R. Soc. Lond.*, *461*, 609–627, doi:10.1098/rspa.2004.1350.
Schoof, C. (2010), Coulomb friction and other sliding laws in a higher order glacier flow model, *Math. Models Methods Appl. Sci.*, *20*, 157–189, doi:10.1142/S0218202510004180.
Scholz, C. H. (2002), *The Mechanics of Earthquakes and Faulting*, Cambridge Univ. Press, Cambridge.
Stocker, T. F., et al. (Eds.) (2013), *Climate Change 2013: The Physical Science Basis. Contribution of Working Group I to the Fifth Assessment Report of the Intergovernmental Panel on Climate Change*, Cambridge Univ. Press, Cambridge and New York.
Tsai, V. C., A. L. Stewart, and A. F. Thompson (2015), Marine ice-sheet profiles and stability under Coulomb basal conditions, *J. Glaciol.*, *61*, 205–215, doi:10.3189/2015JoG14J221.
Weertman, J. (1957), On the sliding of glaciers, *J. Glaciol.*, *3*, 33–38.
Weertman, J. (1964), The theory of glacier sliding, *J. Glaciol.*, *5*, 287–303.
Zoet, L. K., and N. R. Iverson (2015), Experimental determination of a double-valued drag relationship for glacier sliding, *J. Glaciol.*, *61*, 1–7, doi:10.3189/2015JoG14J174.
Zoet, L. K., S. Anandakrishnan, R. B. Alley, A. A. Nyblade, and D. A. Wiens (2012), Motion of an Antarctic glacier by repeated tidally modulated earthquakes, *Nat. Geosci.*, *5*, 623–626, doi:10.1038/ngeo1555.
Zoet, L. K., R. B. Alley, S. Anandakrishnan, and K. Christianson (2013a), Accelerated subglacial erosion in response to stick–slip motion, *Geology*, *41*, 159–162, doi:10.1130/G33624.1.
Zoet, L. K., B. Carpenter, M. Scuderi, R. B. Alley, A. Anandakrishnan, C. Marone, and M. Jackson (2013b), The effects of entrained debris on the basal sliding stability of a glacier, *J. Geophys. Res. Earth Surf.*, *118*, 1–11, doi:10.1002/jgrf.20052.